Contract No.:

This manuscript has been authored by Battelle Savannah River Alliance (BSRA), LLC under Contract No. 89303321CEM000080 with the U.S. Department of Energy (DOE) Office of Environmental Management (EM).

High-performance SO_2-depolarized electrolysis cell using advanced polymer electrolyte membranes

Héctor R. Colón-Mercado,[1] Maximilian B. Gorensek,[2] Cy H. Fujimoto,[3] Aaron Lando,[1] and Benjamin H. Meekins[4]*

[1]Environmental, Materials, and Energy Sciences, Savannah River National Laboratory, Aiken, SC 29808, USA

[2]Advanced Modeling, Simulation, and Analytics, Savannah River National Laboratory, Aiken, SC 29808, USA

[3]Nanoscale Sciences Department, Sandia National Laboratories, Albuquerque, NM 87185-0734, USA

[4]Department of Chemical Engineering, University of South Carolina, Columbia, SC 29208, USA

*Corresponding author: hector.colon-mercado@srnl.doe.gov

Abstract (143 words)

Three different proton conducting polymeric membrane materials (Nafion® 115, Nafion® 212, and sulfonated Diels-Alder polyphenylene [SDAPP]) were evaluated for use in SO_2-depolarized electrolyzers for the production of hydrogen via the hybrid sulfur cycle. Their performance was measured using different water feed strategies to minimize overpotential losses while maintaining high product acid concentration. Both thin membranes (Nafion® 212 and SDAPP) showed performance superior to that of the thicker Nafion® 115. The SDAPP membrane electrode assembly (MEA) performed well at higher acid concentrations, maintaining low ohmic and kinetic overpotentials. Finally, short-term (100-h) stability tests under constant current conditions showed minimal degradation for the SDAPP and Nafion® 212 MEAs. SDAPP MEA performance approached the targets needed to make the hybrid sulfur cycle a competitive process for hydrogen production (product acid concentration $\geq$ 65 wt% H_2SO_4 at $\leq$ 0.6-V cell potential and $\geq$ 0.5 A-cm^{-2} current density).

Keywords: hybrid sulfur (HyS) process; sulfur dioxide-depolarized electrolyzer (SDE); hydrogen production; sulfuric acid production; sulfonated Diels-Alder polyphenylene (SDAPP).

Highlights:

- High water transport across SDAPP membrane allows efficient electrolysis
- Thicker membranes can only operate in well-hydrated environments
- Thin membranes can operate with a wet cathode and dry anode
- High acid concentration (>60 wt%) was produced at potentials < 1 V
- Stable operation observed under moderate operating conditions

1.0 Introduction

The race to lower CO_2 emissions and increase energy efficiency is on-going. With more renewable resources coming on-line that peak at different times of the day, there is a growing need for new technologies to store energy. Because of the chronological, seasonal, and geographical diversity of the available resources, a single technology cannot be expected to fill this need. Fortunately, there is a multitude of ways that energy can be transformed and converted so that it can be stored. One development is the production of hydrogen, as it not only provides convenient chemical energy storage, but it can also serve as a feedstock for many different commodity products [1]. For renewable hydrogen to be competitive with existing hydrogen production technologies, the conversion processes being considered must be comparable in cost to that of the industry standard, steam-methane reforming. The hybrid sulfur (HyS) process has been suggested as one of the alternatives for hydrogen production that could meet this cost target [2-5].

Several requirements need to be satisfied for HyS to be competitive. One of the most important is efficient electrolyzer operation, to take full advantage of the anode depolarizing effect of SO_2. (The standard potential for SO_2-depolarized electrolysis is only 0.158 V, about 13% of that for electrolysis of water, 1.229 V [3].) Technoeconomic analyses (TEAs) have suggested that for HyS to be competitive, the electrolysis process must operate at a potential-current combination of ≤ 0.6 V and ≥ 0.5 A-cm^{-2} while producing acid at a concentration of ≥ 65 wt% H_2SO_4 [3]. However, these values have proven to be hard to achieve. Aside from the original work in the late 1970s - early 1980s [6-8], a number of strategies to improve electrolyzer performance have been pursued in recent years. This includes catalyst development, membrane development, and changes in electrolyzer design and operation.

In the area of catalyst development, various groups have looked at the use of different catalytically active metals such as Pt, Pd, Au, Ir, Ag, PtPd, PtPdAl, PtRu, PtRh, PtCr, PtIr, PtCr, and PtAu supported and unsupported on carbon to lower the overpotential for the SO_2 oxidation reaction [9-19]. However, most of the conclusions for catalyst improvement were derived from measurements of catalyst performance in either

half cells or in electrolysis cells with subpar cell performance. Among the few published results using catalysts other than Pt/C is the recent work by Meekins et al. [16] that shows the performance of Au/C in electrolyzers with low catalyst loadings is superior to Pt/C.

In the area of membrane testing, Elvington, et al. [20] screened the attributes of different families of membranes vs. state-of-the-art Nafion®. Among the proton-conducting materials studied, polybenzimidazole (PBI) and sulfonated Diels-Alder polyphenylene (SDAPP) membranes were identified as suitable for future testing given their high ionic conductivities and ability to operate at high temperatures.

In the area of electrolyzer design and operation, two different approaches (both using Pt catalyst) have been pursued. The first approach utilizes an all-liquid feed system. This was optimized by Steimke et al. [21] However, the all-liquid-fed electrolyzer was found to suffer from mass transport limitations at the catalyst layer, large SO_2 crossover through the Nafion® 115 (N115) membrane, and corrosion of wetted surfaces. In addition, because of test stand materials limitations, it was hard to operate at temperatures above 90ºC. Using an all-liquid-fed system, the best cell performance that could be achieved was 0.73 V at 0.5 A-cm^{-2} and an acid concentration of ~30 wt% H_2SO_4 [21].

To get around the materials issues, Sivasubramanian et al. [22] developed a gas-fed electrolyzer design. With this approach, many of the materials corrosion and SO_2 crossover issues were avoided by feeding anhydrous SO_2 gas to the anode side and water to the cathode side. The electrolysis reaction relied on osmotic pressure-driven water transport across the membrane to get enough water to the anode side. Water flowing from the cathode to the anode counteracted the SO_2 flux from the anode to the cathode. Subsequently, Staser et al. [23] improved cell operation by applying a differential pressure across the membrane and using thinner membranes (Nafion®) to compensate for the limited water transport through the membrane due to osmotic pressure. This caused a significant increase in electrolyzer performance, surpassing that of the liquid-fed cell. Further improvement accrued when Staser et al. [24] replaced Nafion® with SDAPP high-temperature membranes. An SDAPP membrane-equipped gas-fed cell achieved a performance of 0.8 V at 0.5 A-cm^{-2} at an approximate acid concentration of 45 wt% H_2SO_4.

While this was a significant breakthrough, the performance was still far from the TEA target. An additional increase in pressure allowed the cell to reach a performance of 0.7 V at 0.5 A-cm^{-2} using Nafion® 212 (N212) membrane, although the acid concentration was reduced to ~35 wt% H_2SO_4 [25]. In 2017, Garrick et al. used sulfonated PBI (s-PBI) membranes in a gas-fed electrolyzer, allowing higher temperature operation than had previously been possible [26]. The electrolyzer was operated at up to 120°C, achieving a best-yet performance of 0.65 V at 0.5 A-cm^{-2}, although the product acid concentration was only around 25 wt% H_2SO_4.

In this work, we take a closer look at the operating conditions of the electrolyzer using standard Pt/C electrodes that have been optimized for SO_2 electrolysis. We focus on standardizing flowrates to industrially realistic conditions (low stoichiometric flows), and we evaluate the cell performance at acid concentrations relevant to the TEA predictions, taking into account various operating conditions such as wet or dry cathode, wet or dry anode, measuring water crossover, and evaluating the optimal operating conditions for each of the three different membranes N115, N212, and SDAPP.

2.0 Materials and methods

2.1 Materials

Forty-six wt% Pt on high surface area carbon (TEC10E50E, TANAKA Kikinzoku Kogyo), isopropyl alcohol (ACS, Acros Organics), Nafion® ionomer (D-520, Alfa Aesar), sulfur dioxide (anhydrous, Matheson), carbon cloth (PRIMEA, W. L. Gore and Associates, Inc.), and Nafion® membranes (Nafion® 115 and Nafion® 212, FuelCellStore) were all used as received. Dichloromethane, dimethyl sulfoxide, and chlorotrimethylsilyl sulfonate were purchased from Aldrich. Sulfonated Diels Alder Poly(phenylene) was prepared following procedures previously reported [27].

2.2 Overpotential calculations

2.2.1 Reversible cell potential

The reversible cell potential can be calculated using the Nernst equation when the activities of the participating species at the anode and cathode are known [28]. In the absence of direct measurements, a material balance model of the experimental electrolysis cell that incorporates a rigorous thermodynamic model of the participating species can be used to predict gas and liquid phase compositions at the electrodes. An Aspen Plus material and energy balance model of the experimental electrolysis cell (see Figure 1) was built similar to the one published by Gorensek et al. [29] Proton transport and osmotic flux of water were simulated with separation blocks (SDE-MEAP and SDE-MEAW, respectively) and the oxidation of SO_2 to H_2SO_4 replicated with a stoichiometric reactor block (SDE-RX). Phase equilibria and species concentrations and activities were calculated for each set of experimental conditions with flash calculations of the anode and cathode product streams (SDE-ANOD and SDE-CATH, respectively), using the symmetric electrolyte NRTL activity coefficient model for the highly non-ideal $SO_2 – H_2SO_4 – H_2O$ system developed by Kaur et al. [30] This allowed the reversible potentials to be calculated as shown by Kaur et al. [30]

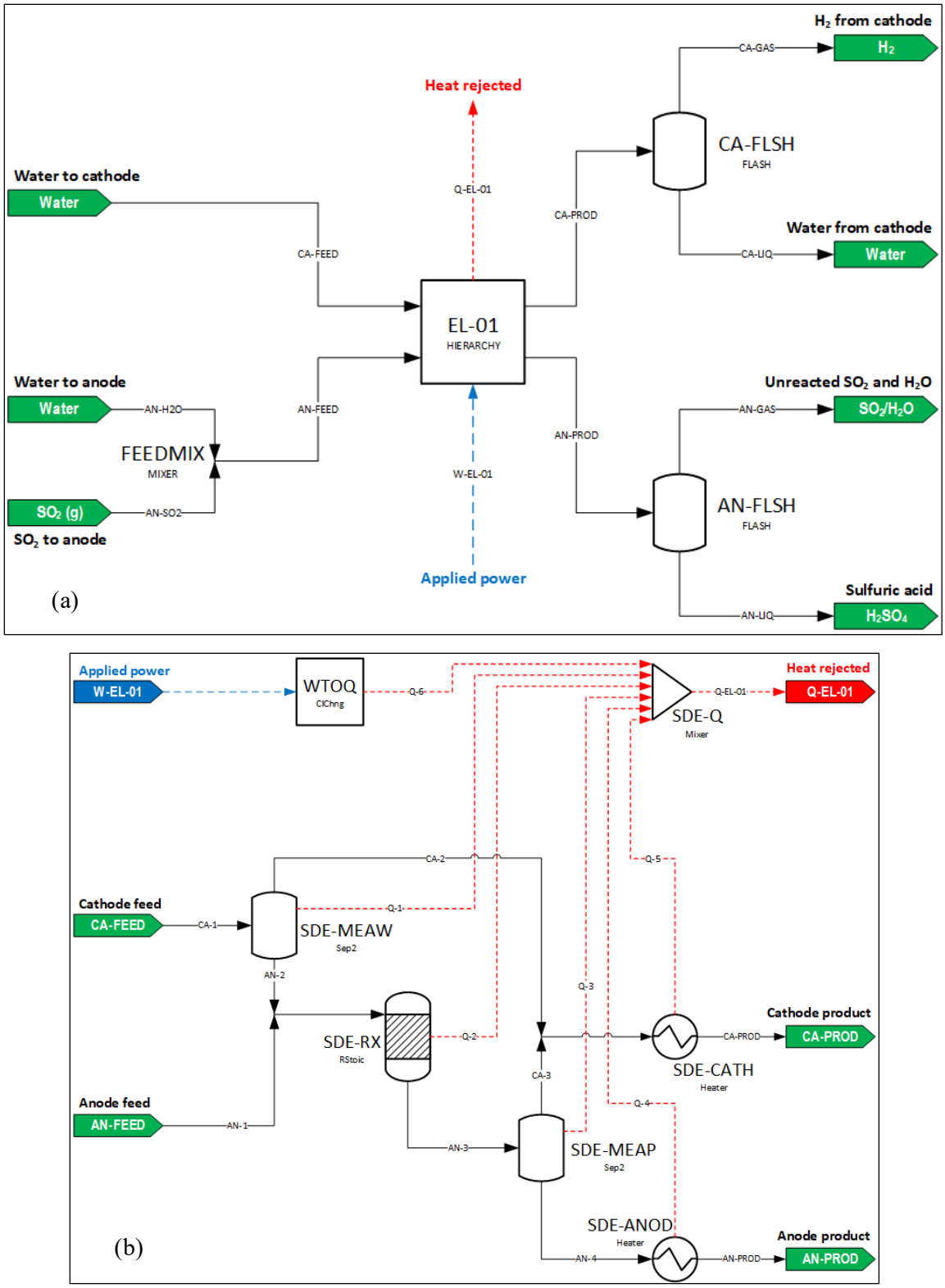

Figure 1. *Aspen Plus hierarchical model of the experimental electrolysis cell: a) electrolyzer with feed and product stream connections; b) electrolyzer hierarchy block internal structure.*

2.2.2 Ohmic overpotential

The ohmic component of the cell potential was determined experimentally from the high frequency (ca. 11 kHz) resistance of the cell at the operating current. This was measured by galvanostatic electrochemical impedance spectroscopy with an applied perturbation current of 100 mA.

2.2.3 Kinetic overpotential

The kinetic component was calculated by subtracting the ohmic overpotential and the thermodynamic reversible potential from the operating cell potential. This term includes mass transport limitations that, while small, do contribute to the overpotential.

2.3 Electrolyzer

2.3.1 Membrane electrode assembly fabrication

Membrane electrode assemblies (MEAs) were prepared by direct spraying of the catalyst ink onto the carbon cloth. The ink was prepared by mixing 400 mg catalyst with 25 g deionized water, followed by 6.8 g isopropanol. After ultrasonically mixing for 5 min, 1.5 mL Nafion® ionomer was added. The ink was then sonicated in an ice bath for 1 h to avoid dispersion heat-up. Afterwards, the ink was loaded to an automated ultrasonic sprayer (Prism-400BT, Ultrasonic Systems, Inc.), where it was mixed for an additional 30 min. The carbon cloth was placed on a vacuum heated plate (at 100 ºC) where a coating area of 100 cm^2 with the desired loading was deposited. All 5-cm^2 electrodes were cut from the same Pt coated carbon cloth to avoid variations in the results. The anode and cathode catalyst loadings were maintained at 0.5 mg Pt cm^{-2}. The MEA was assembled by hot pressing a 254 µm thick PTFE gasket followed by the carbon cloth, membrane, carbon cloth, and another 254 µm thick PTFE gasket at a pressure of 50 kg cm^{-2} (gasketed total area) for 3 min at 125 ºC. After hot pressing, the MEA was allowed to cool to room temperature. The finished MEA was placed between 25-cm^2 single serpentine graphite flow fields and assembled in a cell fixture (Scribner Associates, Inc.). The gaskets ensure that only 5 cm^2 of active surface area are exposed to the operating conditions. This configuration allows for internal conditioning of the feeds prior to

reaching the active surface area. The bolts holding the cell together were tightened with a torque of 4.5 N-m each (6 bolts total). Finally, the cell fixture was connected to a custom test station. Figure 2 shows a diagram of the custom test station used for the electrochemical characterization.

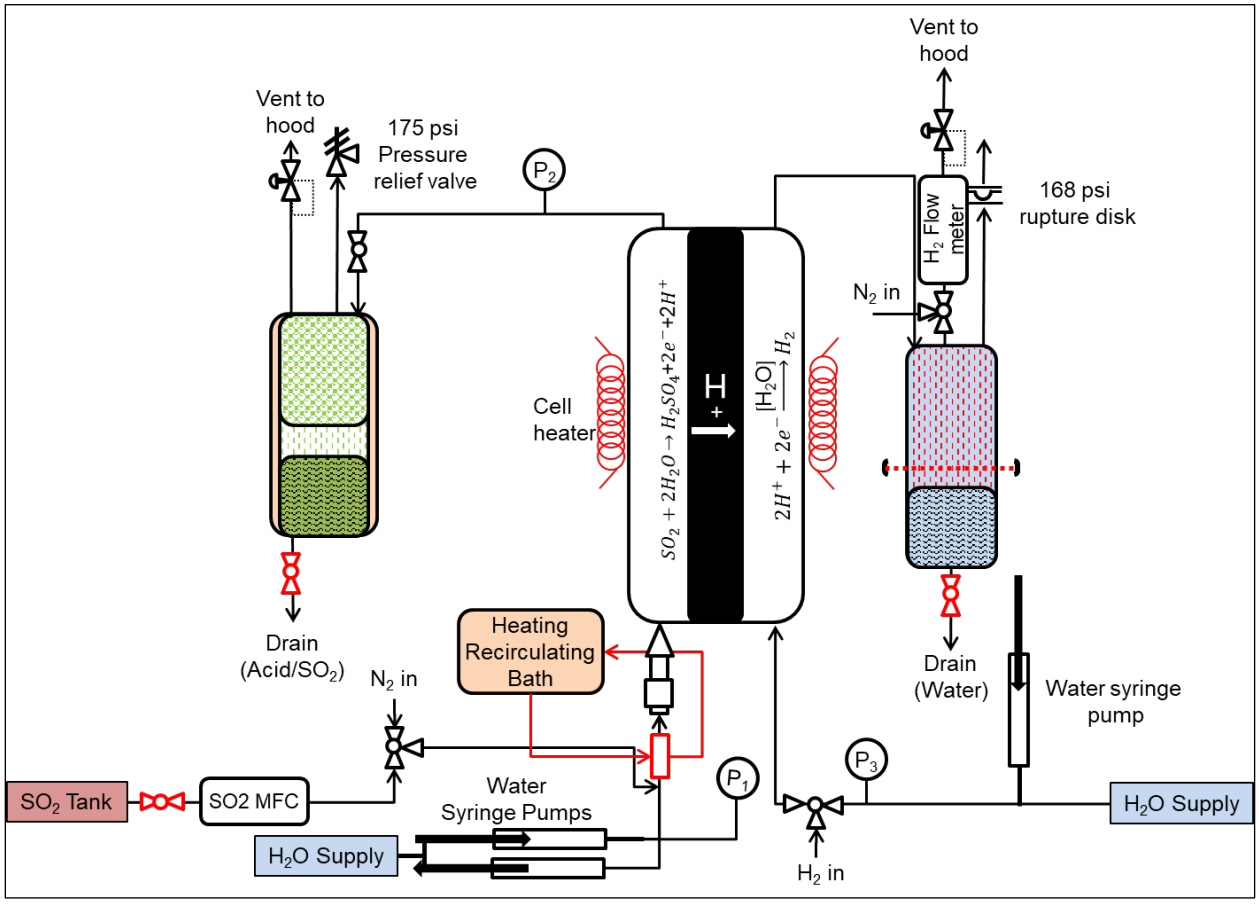

Figure 2 ***Custom test station for the evaluation of performing electrochemical characterization of the MEAs.***

2.3.2 Cell break-in

Before testing, the anode was first purged with N_2 at 126 standard cm^3 min^{-1} (sccm) while the cell and the delivery lines were heated to 96 ºC. Once at temperature, a flow of 0.29 mL min^{-1} H_2O mixed with ~ 100 sccm H_2 was started to the cathode and a flow of 126 sccm N_2 plus 0.6 mL min^{-1} H_2O was started to the anode. Steady all-vapor conditions were achieved at the anode by mixing the gas flow with the water flow using a "T" connection and then passing the mixture through a 1-m long heated line. The electrochemical active surface area of the anode was measured by cycling between 0.05 V and 1.1 V vs DHE (Dynamic Hydrogen Electrode) at a scan rate of 20 mV s^{-1}. Once stable voltammograms were collected, the flow of

H_2 to the cathode was stopped and a voltage of 0.95 V was applied using a high current potentiostat (HCP-803, Biologic). The anode feed was switched to 126 sccm SO_2. Once steady state currents were observed, the break-in of the cell was completed by performing a cathodic scan from 0.95 V to 0.65 V at a rate of 0.1 mV s^{-1}. The scan range was chosen to prevent the formation of sulfur on the cathode at the low potential limit or catalyst degradation at the high potential limit.

2.3.3 Constant current experiments

After break-in, the cell was kept under constant voltage and the SO_2 feed (24 sccm at 500 mA-cm^{-2} or 50 sccm at 1000 mA-cm^{-2}; 1.4 stoichiometric ratio) and water feed to the anode were adjusted to yield the desired acid concentration. The cell was operated with (0.29 mL min^{-1}) and without water feed to the cathode. Once stable conditions were achieved (< 0.5% change per min), constant current control was applied and only the temperature was varied, starting at 85ºC and increasing up to 110ºC. Each data point was collected only after waiting for 30 min of stable operation. Additionally, after each temperature set measurement (85 ºC-110 ºC), a cathodic scan (0.95 V to 0.65 V, at a scan-rate of 0.1 mV s^{-1} with a flow of 126 sccm of SO_2 plus 0.6 mL min^{-1} of H_2O to the anode and 0.29 mL min^{-1} H_2O to the cathode) was redone to ensure no MEA performance degradation. To prevent catalyst and hardware degradation, the cell potentials were maintained below 1.1 V. During the constant current runs, water diffusion due to osmosis from the hydrogen side was measured by collecting the water coming out of the cell in a cooled graduated cylinder for 10 min. The difference in the cathode water flow (in-out) was used to calculate the water transported to the anode. The acid concentration was calculated from the anodic reaction, $SO_2 + 2H_2O \rightarrow H_2SO_4 + 2H^+ + 2e^-$, assuming 100% faradaic efficiency and accounting for the water diffused from the cathode through the membrane. A material balance calculation was chosen over direct measurement of the acid concentration to avoid inaccuracies due to dissolved SO_2 that can cause deviations in density or titration measurements. It is important to note that all results were reproducible except for the runs at 110 ºC, which became noisy. While the noise could be eliminated by operating at higher back pressures, operating under pressure or using a pressure differential across the cell was outside the scope of the present study and only

data collected at atmospheric pressure are discussed here. Therefore, results at 110ºC are presented, when available, only to show the trend.

2.3.4 SO_2 crossover measurement

SO_2 crossover has been previously measured electrochemically in various membranes [24]. To carry out the measurement for this work, the cell was operated as usual, with water flowing into the cathode (serving as the working electrode) and either N_2 or SO_2 mixed with water into the anode (serving as the counter/reference electrode). The working electrode was polarized to 0.31 V above equilibrium conditions to convert any SO_2 crossing over through the membrane from the counter/reference side to H_2SO_4. In a typical experiment, the N_2-water mixture was purged on the counter/reference side at a rate of 24 sccm (same gas flowrate as used in the 500 mA-cm^{-2} constant current runs) with 0.6 mL-min^{-1} of water, while water flowed through the working side at 0.29 mL-min^{-1}. Once the cell temperature was stable, a potential of 0.31 V was applied to the working side. After the current decayed to negligible values, the N_2 was switched to SO_2. Because the applied potentials were high enough to oxidize the SO_2 crossing over, the current produced could be directly correlated to SO_2 flux. After the current stabilized, the SO_2 was switched back to N_2 and the temperature was increased. All measurements were taken after waiting at least 30 min between changes in temperature. The measured SO_2 crossover represents the worst-case scenario, as in typical cell operation most of the SO_2 will be consumed prior to reaching the membrane. Additionally, after the measurement a cathodic scan (0.95 V to 0.65 V, at a scan-rate of 0.1 mV s^{-1} with a flow of 126 sccm of SO_2 plus 0.6 mL min^{-1} of H_2O to the anode and 0.29 mL min^{-1} H_2O to the cathode) was redone to ensure no MEA performance degradation.

2.3.5 Short-term testing

Short-term stability was evaluated for fresh MEAs after break-in at similar conditions of acid concentration, temperature, and current density. The test conditions were selected to allow equal comparison among the membranes, while avoiding high operating voltages that can cause fast catalyst degradation. All tests were

performed at 100 ºC and at a current density of 500 mA cm^{-2}. The water input was adjusted so that the real acid concentration produced (considering the water stochiometric flow to the anode plus water crossing from the cathode side) was nominally at 40 wt%. For the MEA with N115 membrane, water was fed at 0.29 mL min^{-1} to the cathode and an anode water stoichiometric flow was chosen to yield 50 wt% H_2SO_4 (assuming no water crossover from the cathode side). For the MEA with N212 membrane, water was fed at 0.29 mL min^{-1} to the cathode, and an anode water stoichiometric flow was chosen to yield 60 wt% H_2SO_4 (assuming no crossover from the cathode side). Finally, for the MEA with SDAPP membrane, water was fed at 0.29 mL min^{-1} to the cathode and no water to the anode. The SO_2 flow was maintained at 24 sccm.

3.0 Results and discussion

The polarization curves, after break-in, can be observed in Figure 3a for the MEAs fabricated with the different membranes. As expected, the cell potential decreases with membrane thickness. However, when MEAs with membranes of similar thickness are compared, it is obvious that the SDAPP membrane shows higher performance. The observed difference in performance can be attributed solely to the membrane as the cyclic voltammograms shows negligible differences in the electrochemical surface area, Figure 3b. This is expected, as all the MEAs were fabricated using the same electrodes. Analysis of the hydrogen under potential deposition peak [31] shows an average electrochemical Pt surface area after baseline correction of 55 $m^2\ g_{Pt}^{-1}$ for all the electrodes (N115: 55.17 $m^2\ g_{Pt}^{-1}$, N212: 55.20 $m^2\ g_{Pt}^{-1}$, SDAPP: 55.83 $m^2\ g_{Pt}^{-1}$). It is important to note that the electrochemical surface area is lower than expected due to sulfur impurities from the gas lines and cell hardware accumulated from previous experiments attaching to the Pt surface. This observation is further confirmed by the high oxidation peak at potentials above 0.8 V, where sulfur species are electrochemically oxidized [32].

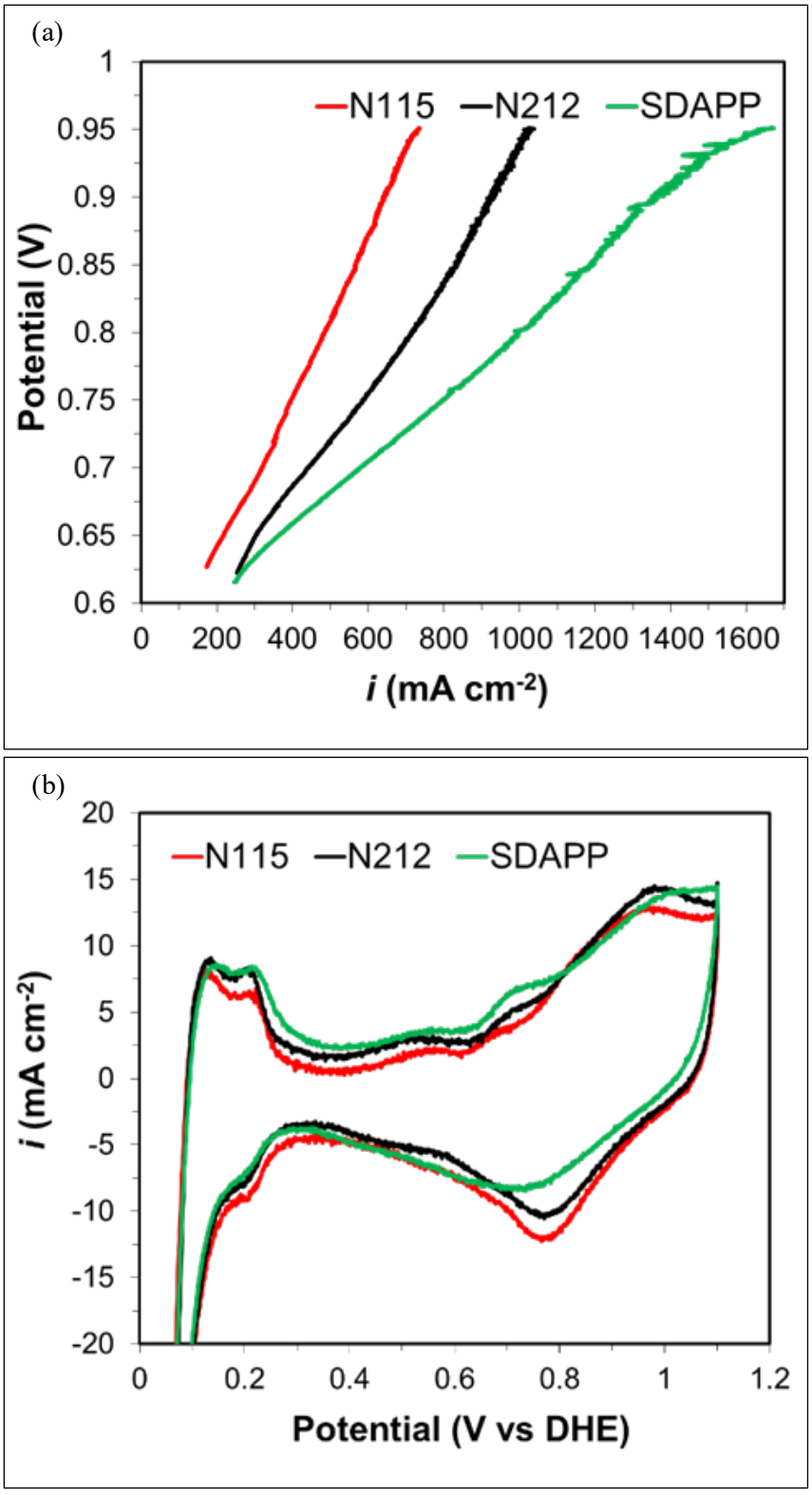

Figure 3. *a) Cathodic scan of the SO_2 electrolysis cell at 95°C after break-in under constant water flow to the anode and cathode, and constant SO_2 flow. Polarization scan performed at 0.1 mV s^{-1}. b) Cyclic voltammogram of the anode. Scan performed at 20 mV s^{-1}.*

SO_2 transport across the membrane was also evaluated at various temperatures. Figure 4 shows the crossover current density as a function of cell temperature. The overall trend for all three membranes shows that as temperature increases, the SO_2 crossover current decreases. This behavior is expected as the SO_2 solubility and hydration of the membrane decreases with increase in temperature [33] without an increase in the system pressure. At low temperatures, the observed SO_2 crossover currents are in the vicinity of reported values for N115 [24]. The small difference between the literature-reported crossover currents and the observed currents in this study could be explained by the difference in gas flowrate during the measurement. In the present work, the flowrates are low and representative of normal cell operation, while the literature flowrate values were not reported. Based on data not reported in the present work, it has been observed that when the SO_2 flowrates were high, the membrane surface exposed to the gas stream dried out and the SO_2 crossover current decreased. This is expected as the SO_2 must first dissolve in the water channels of the membrane to be able to cross over. As observed in Figure 4, the crossover currents as function of temperature for N115 and N212 are not parallel and the ratio of the crossover currents is not 5:2 as one would expect based on the membrane relative thickness. Additionally, the SO_2 crossover profile of the SDAPP membrane is different compared to that of the Nafion®-based membranes. This could be due to the difference in the membrane backbone and hydration characteristics of the SDAPP [34]. However, it is important to note that the crossover measurements were evaluated under rest conditions. When the cell is in operation, the amount of SO_2 reaching the membrane will be reduced. Therefore, a membrane that operates at higher current densities will be expected to have lower SO_2 concentration reaching the membrane and crossing over to the cathode side.

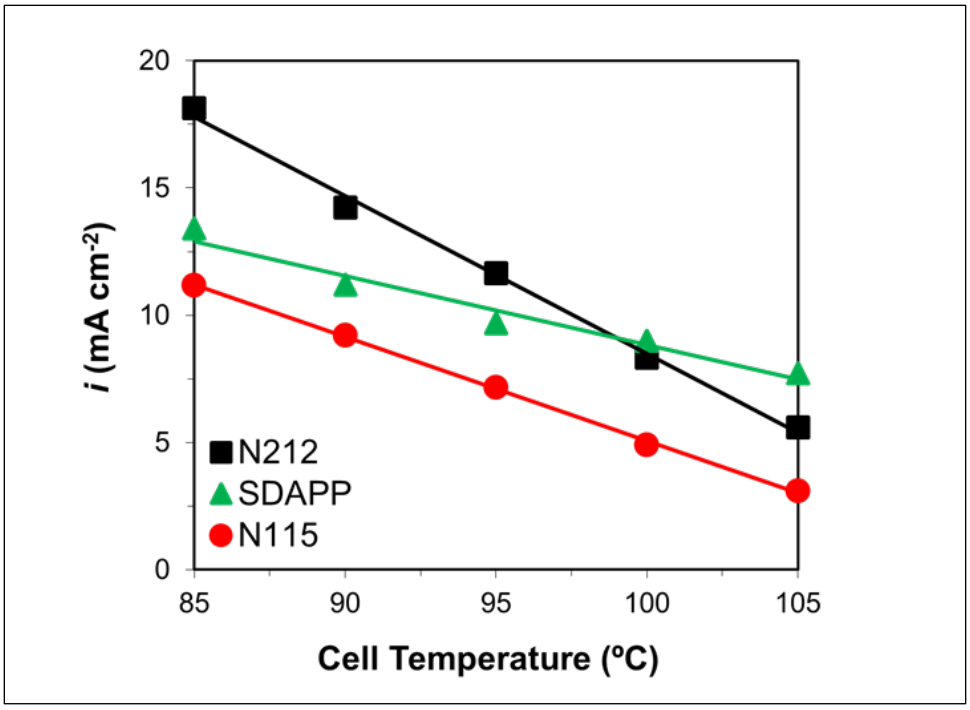

Figure 4. ***SO_2 crossover current density as a function of temperature.***

Cell performance was evaluated for various operating conditions to understand the limitations of and optimal operating conditions for each MEA. It would be expected that although the gas diffusion electrodes are identical, differences in membrane properties can impact the local environment (acid concentration) and therefore affect the overall cell performance [15, 16, 28]. Additionally, higher IR losses (ohmic losses) arising from the membrane will limit the maximum current for safe potential operation (set to 1.1 V) with the carbon-based cell components. Figure 5a shows the cell overpotentials as a function of cell temperature for the cell operated with water feed on both sides and a current density of 500 mA-cm^{-2}. The summation of the overpotentials corresponds to the total cell operating potential. As observed in Figure 5a, all MEAs were able to perform at cell potentials at or below 1.1 V. Figure 5b helps focus the discussion on the kinetic and ohmic results. The results for the different temperatures are presented as a single point mean value. The change in the values from the various temperatures is presented in the form of error bars (standard deviation) around the mean values. As expected, the kinetic overpotentials are similar between the different MEAs and influenced by the cell temperature, as represented by the large error bars around the mean values

(a decrease in kinetic overpotential is observed in Figure 5a as the temperature increases). This behavior is expected as the Pt catalyst kinetics are only mildly affected by acid concentration.[16] One interesting point is that the error bars are smaller at lower anode water stoichiometry, indicating a decreased dependence on temperature. The kinetic values from the N115 MEA are slightly higher than those from the thinner membranes, which indicates that they include local mass transport limitations, most likely arising from reduced water diffusion from the cathode side.

The ohmic losses show a major dependence on the membrane thickness; while in theory the temperature and hydration will influence the ohmic losses, those effects are only observed for the thicker N115 membrane (positive slope of ohmic losses with increasing acid concentration and error bars around the mean values). This result is expected as hydration of the cell is influenced by water diffusion from the cathode side which affects the local environment. In turn, these results support the kinetic overpotential observation for the N115 MEA, which contains a small contribution from water mass transport resistance. The ohmic loss behavior for the thinner membranes shows little effect due to temperature of operation and water stoichiometry at the anode, a fact demonstrated by the lack of error bars and the similar mean values at the different water stoichiometries. Overall, the SDAPP MEA has lower resistance due to the inherent properties of the membrane as can be observed from the overall lower ohmic losses at the different acid concentrations.

The thermodynamic cell potential (Figure 5a) is heavily influenced by acid concentration, pressure, and temperature; however, the effect of acid concentration (hydration influenced due to water crossover) plays a major role in the thermodynamic potential for the operating conditions under consideration. As expected, as the acid concentration in the product increases (influenced by the water diffusion from the cathode and water stoichiometry at the anode), so does the thermodynamic potential. The summation of these losses shows the delicate balance that needs to be achieved in order to maximize the electrolyzer and overall hybrid sulfur cycle efficiency.

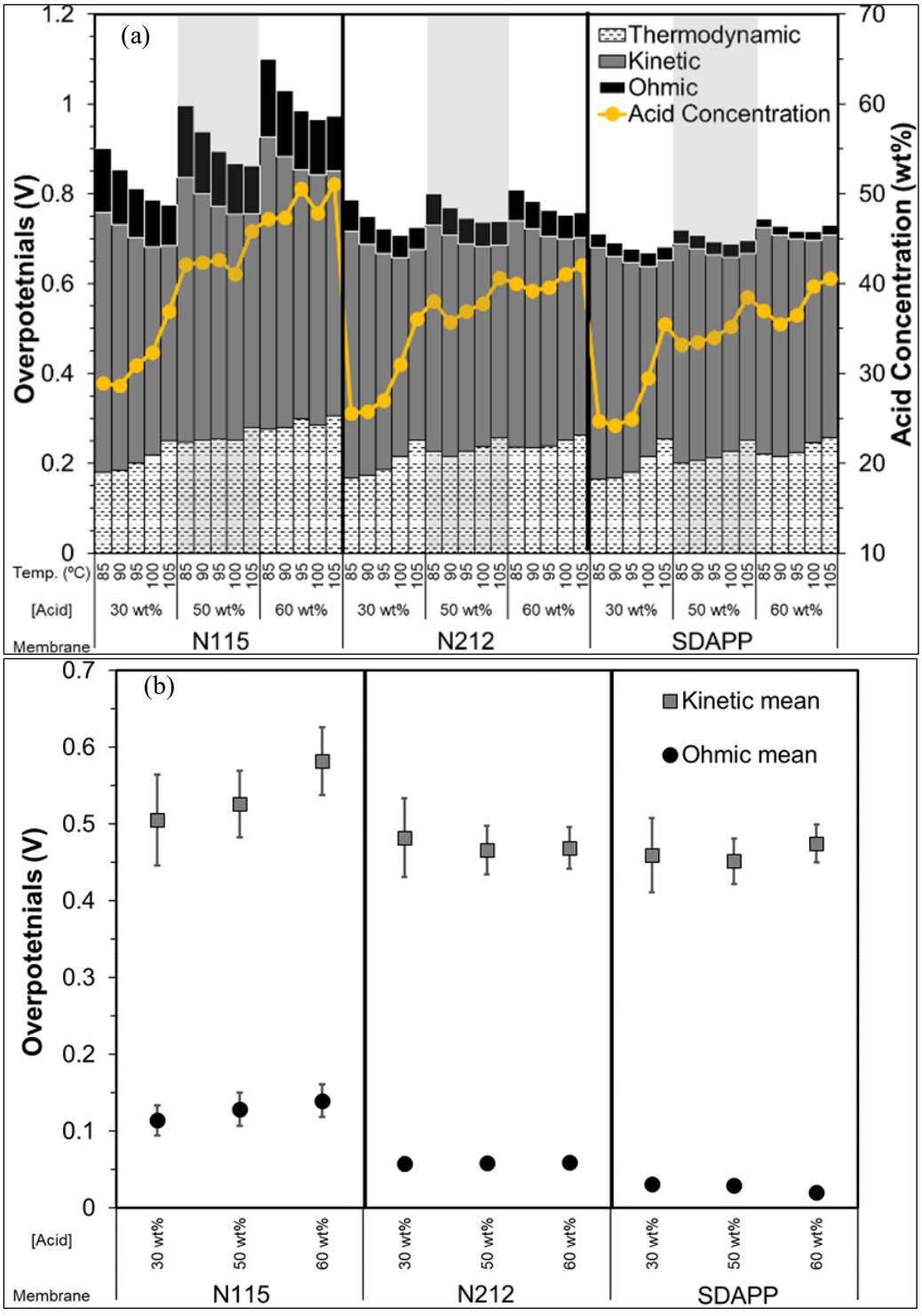

Figure 5. ***a) Electrolyzer results for MEAs with N115, N212, and SDAPP membranes operated at 500 mA cm^{-2} with constant water flow at the cathode and various anode water inputs to produce 30, 50 and 60 wt% acid as a function of temperature. The sum of the overpotentials corresponds to the total cell voltage. Acid concentration is represented by the line for the different operating conditions taking in consideration water crossover from the cathode and the operating conditions of cell temperature and pressure. b) Kinetic and ohmic mean values for constant water stoichiometry. Error bars indicate the standard deviation relative to the change due to temperature effect.***

Figure 6a shows cell operation under similar conditions including water feed on both sides of the cell, but at a current density of 1000 mA-cm^{-2}. Operation at the higher current density pushes the mass transport limitations and material limits due to high potential operation. Stable operation below 1.1 V was only achieved for MEAs with N212 at 30 wt% and for MEAs with SDAPP membranes. Due to the fact that the performance is evaluated far from equilibrium and because of the low mass transport losses in the system, the calculated kinetic overpotentials (Figure 6b) are only slightly higher than the values in Figure 5b. The N212 MEA shows the highest mean kinetic overpotential which demonstrates that the local environment of the MEA is water-limited. This fact is further demonstrated by the steady increase in acid concentration. The ohmic loss contribution in Figure 6b shows that the ratio between the SDAPP and N212 values is similar to the value reported in Figure 5b. Additionally, the larger error bar observed around the ohmic mean value for the N212 MEA supports the conclusion that the MEA is operating under increased localized water mass transport resistance. The lack of visible error bars around the ohmic mean values for the SDAPP data clearly shows the advantage of the SDAPP membrane by allowing lower ohmic losses through higher water availability at the catalyst layer interphase due to higher water crossover. The SDAPP MEA allows lower operating potentials while still producing higher acid concentrations. Under similar product acid concentration, the SDAPP MEA operated at 1000 mA cm^{-2} (Figure 6a) shows lower cell potentials than the N115 MEA operated at 500 mA cm^{-2} (Figure 5a). The lower ohmic losses in the SDAPP MEA offset the higher thermodynamic potentials due to the production of more concentrated acid.

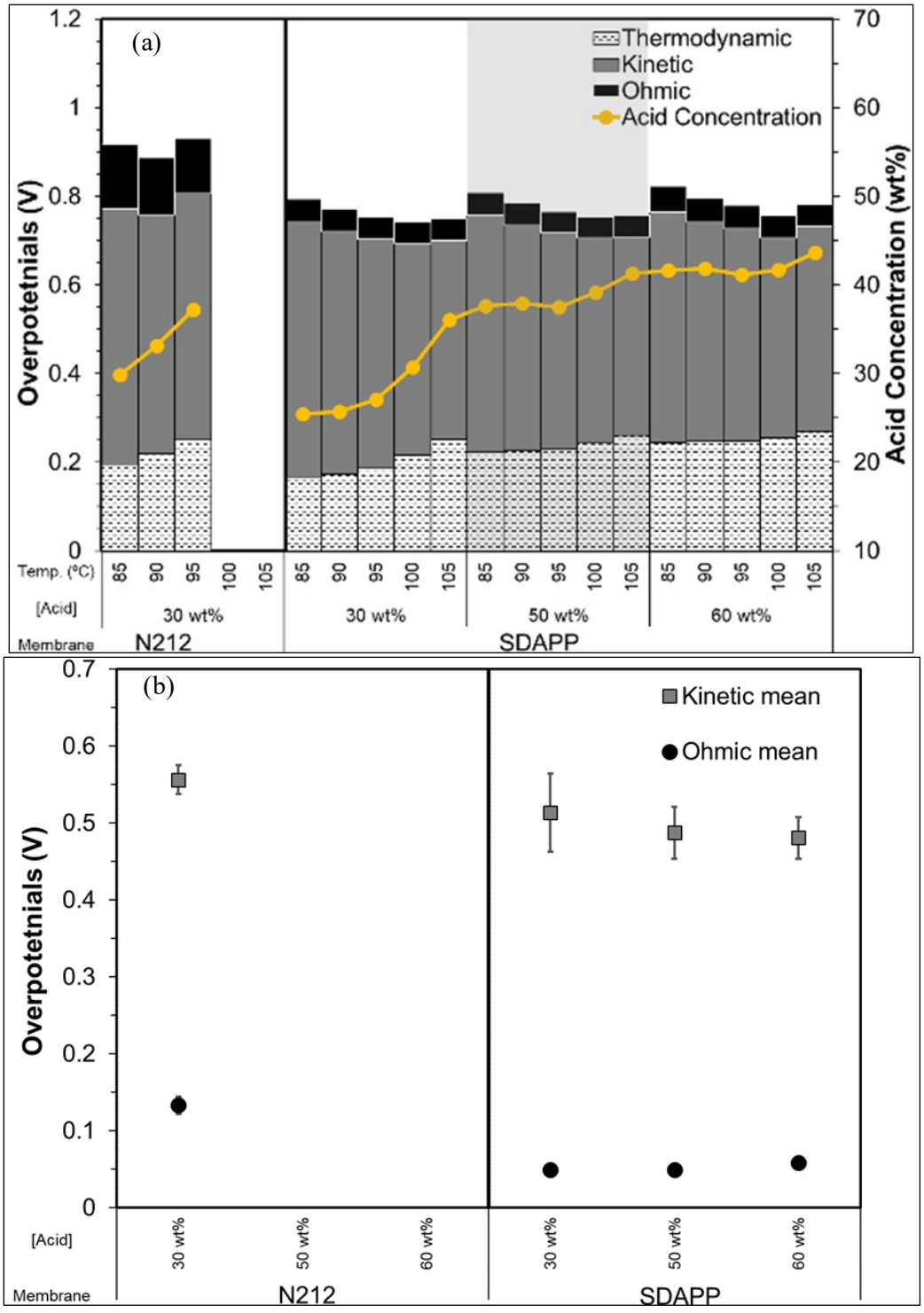

Figure 6. ***a) Electrolyzer results for MEAs with N212 and SDAPP membranes operated at 1000 mA cm^{-2} with constant water flow at the cathode and various anode water inputs to produce 30, 50 and 60 wt% acid as a function of temperature. The sum of the overpotentials corresponds to the total cell voltage. Acid concentration is represented by the line for the different operating conditions taking in consideration water crossover from the cathode and the operating conditions of cell temperature and pressure. b) Kinetic and ohmic mean values for constant water stoichiometry. Error bars indicate the standard deviation relating to the change due to temperature effect.***

In order to eliminate the water crossover contribution to the MEA performance, Figure 7a shows cell potential components as functions of temperature with water fed only on the anode side and at a current density of 500 mA cm^{-2}. Stable operation below 1.1 V was only achieved for MEAs with N212 and with SDAPP. It is important to note that due to the limited amount of data under these operating conditions, the mean values and the error bars do not completely cover the entire temperature range. Eliminating the crossover of water from the cathode results in a very strong potential dependence on temperature and water stoichiometry as shown by the large error bars around the kinetic mean values (Figure 7b). Additionally, the kinetic mean values (Figure 7a – N212: mean voltage of 511 mV [578 mV@85ºC to 445 mV@105ºC] for 30 wt%; SDAPP: mean voltage of 486 mV [537 mV@85ºC to 431 mV@105ºC] for 30 wt% and a mean voltage of 490 mV [637 mV@85ºC to 395 mV@105ºC] for 50 wt%) are slightly higher at the lower temperatures, but they are reduced as the temperature of the cell increases to values only slightly higher than previously observed values (Figure 5a – N212: mean voltage of 482 mV [549 mV@85ºC to 424 mV@105ºC] for 30 wt%; SDAPP: mean voltage of 459 mV [516 mV@85ºC to 398 mV@105ºC] for 30 wt% and a mean voltage of 452 mV [489 mV@85ºC to 415 mV@105ºC] for 50 wt%). This effect could be related to a limit in the water availability at the local membrane-electrode interphase since all the water must diffuse through the anode and reach the catalyst layer. In addition, the water coming to the catalyst layer will encounter the concentrated acid leaving the reaction sites. This could result in water absorption in the acid and reduce the free water reaching the catalyst site, resulting in lower local water availability. Interestingly, the ohmic overpotentials are similar to those observed under wet anode and wet cathode conditions for the SDAPP MEA while the ohmic losses are higher for the N212 MEA (Figure 7b vs Figure 5b values), indicating that the SDAPP membrane is not as affected by water availability as the kinetics and mass transport to the catalyst layer.

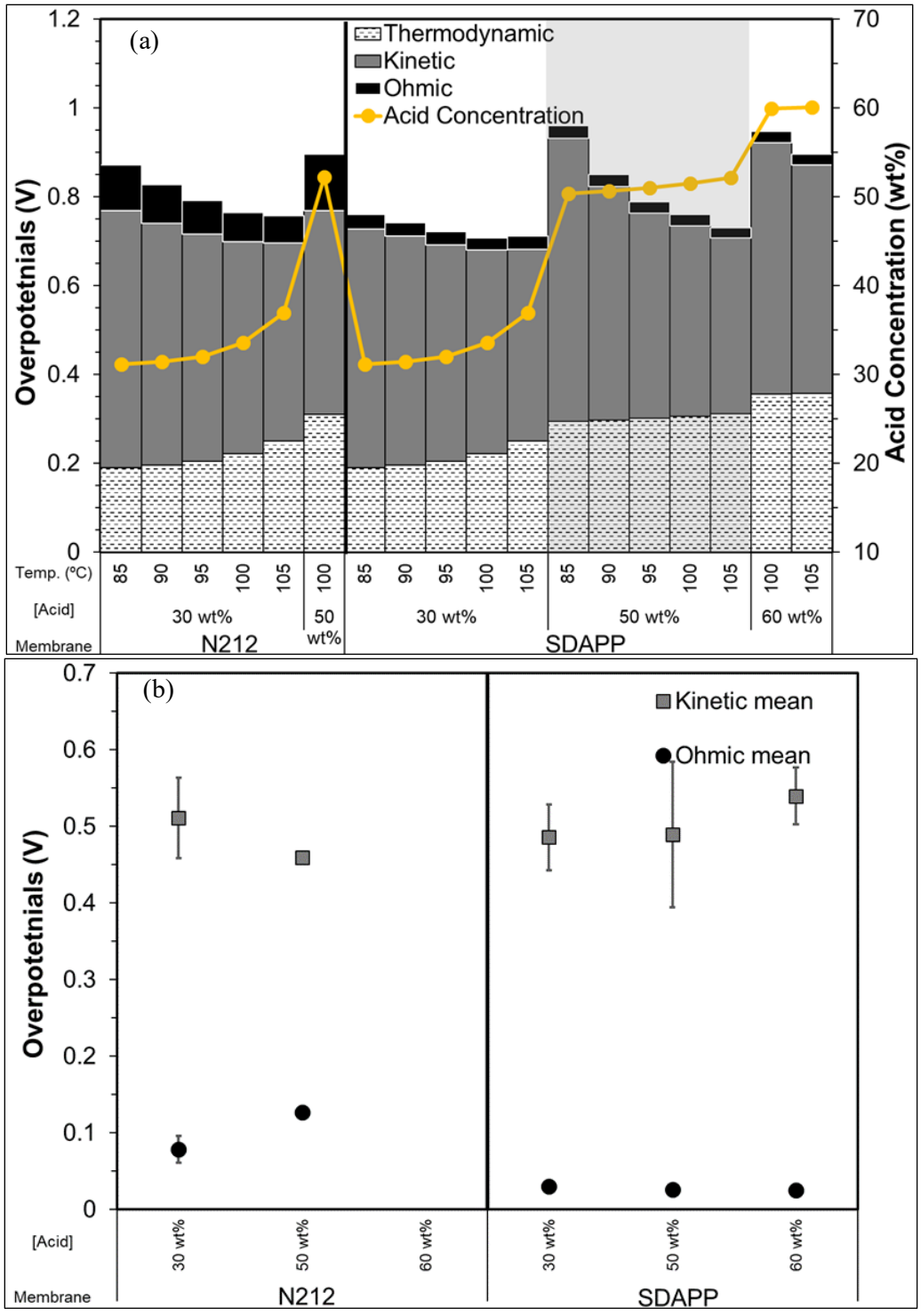

Figure 7. ***a) Electrolyzer results for MEAs with N212 and SDAPP membranes operated at 500 mA cm^{-2} with a dry cathode and various anode water inputs to produce 30, 50 and 60 wt% acid as a function of temperature. The sum of the overpotentials corresponds to the total cell voltage. Acid concentration is represented by the line for the different operating conditions of cell temperature and pressure. b) Kinetic and ohmic mean values for constant water stoichiometry. Error bars indicate the standard deviation relating to the change due to temperature effect.***

It is obvious from the higher acid concentration that the thermodynamic potentials reach higher values than those observed in previous experiments. Overall, these results show that the local water availability at the anode catalyst layer is very important to the electrode performance. Additionally, the results indicate that water diffusion is extremely important for efficient cell operation.

The contribution of water diffusion to the cell performance is shown in Figure 8, where the electrolyzer performance is measured with water fed only through the cathode side and anhydrous SO_2 at the anode side. While this strategy was previously studied by Staser et al. [24, 25] with the use of a pressure differential to promote water transport from the cathode to the anode, here the performance is evaluated without a pressure gradient and relies solely on water activity/concentration as the driving force. The potential relationships for SDAPP and N212 MEAs are shown in Figure 8a for 500 mA cm^{-2} for both MEAs and at 1000 mA cm^{-2} for the SDAPP MEA. Surprisingly, the MEAs operated with a dry anode show improvement in performance, especially when considering the higher acid concentration product as compared to when water is flowing into both electrodes. It is obvious from the acid concentration that it is influenced by temperature, indicating that the water diffusion increases with temperature. It is also noted that higher acid concentrations are attained, exceeding 65 wt% for the SDAPP MEA.

Figure 8b shows that the ohmic overpotential is consistent with the previous data presented. However, the kinetic overpotential is lower under these operating conditions than under the different operating conditions studied. In addition, there is less variation with temperature as indicated by the smaller error bars. The lower kinetic losses could be attributed to lower mass transport resistance since the water is readily available from the cathode to the anode membrane-catalyst layer interphase, and therefore is not affected by acid product or SO_2 transport to the anode. Table 1 summarizes the mean ohmic and kinetic losses from the different conditions and shows that the lowest values are obtained by operating at dry anode-wet cathode conditions with a SDAPP membrane. These data suggest that it is possible to further reduce the ohmic and kinetic losses by operating at higher temperatures and under pressurized conditions to maintain water availability in the liquid phase at the MEA.

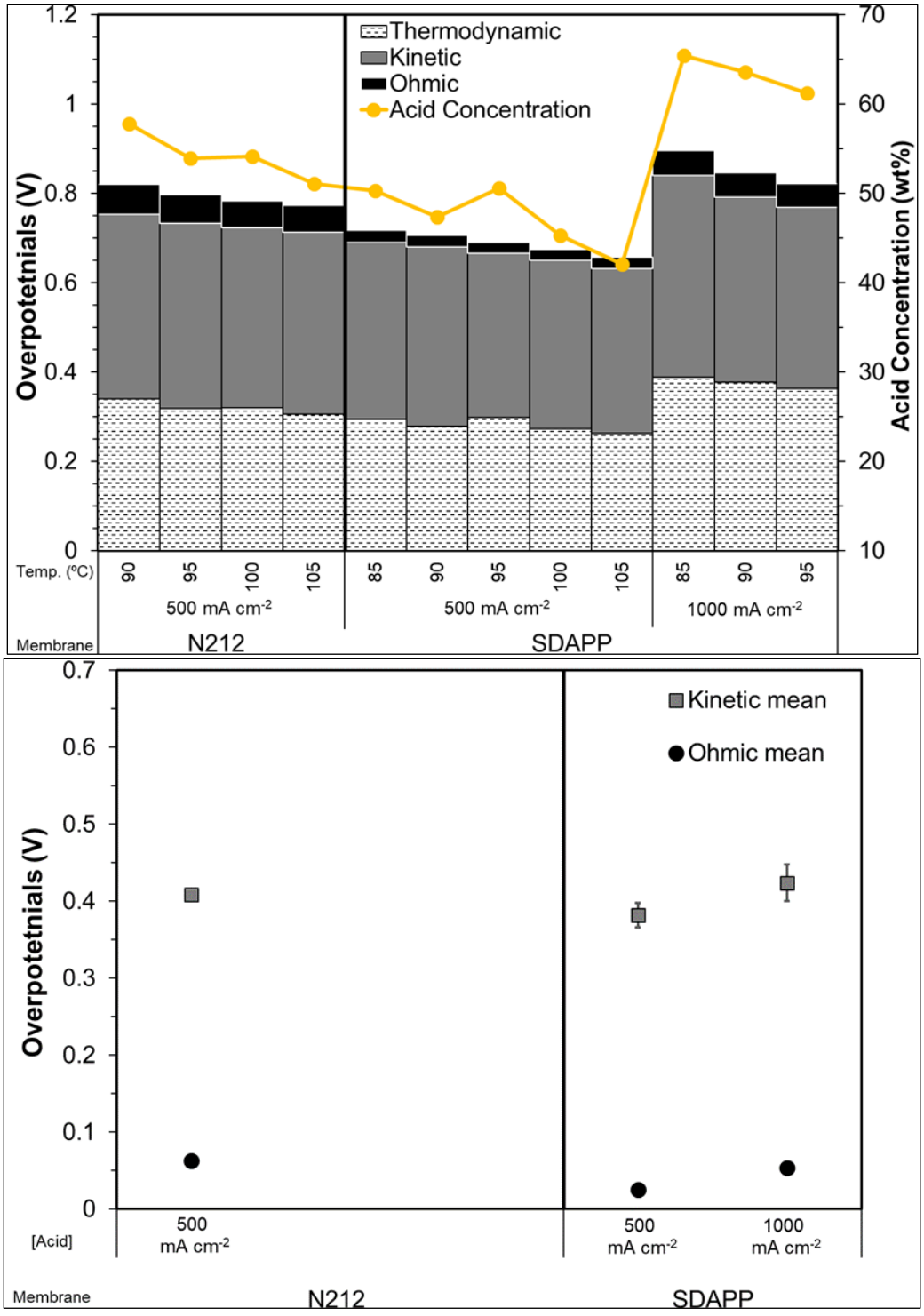

Figure 8. ***a) Electrolyzer results for MEAs with N212 and SDAPP membranes operated at 500 mA cm^{-2} and 1000 mA cm^{-2} with constant water flow at the cathode and dry SO_2 as a function of temperature. The sum of the overpotentials corresponds to the total cell voltage. Acid concentration is represented by the line for the different operating conditions taking into consideration water crossover from the cathode and the operating conditions of cell temperature and pressure. b) Kinetic and ohmic mean values for constant water stoichiometry. Error bars indicate the standard deviation relating to the change due to temperature effect.***

Table 1. ***Summary of mean kinetic loss and mean ohmic loss values for the different conditions evaluated.***

		Loss (V)							
		500 mA cm^{-2} wet anode//wet cathode		1000 mA cm^{-2} wet anode//wet cathode		500 mA cm^{-2} wet anode//dry cathode		dry anode//wet cathode (mA cm^{-2})	
		Ohmic	Kinetic	Ohmic	Kinetic	Ohmic	Kinetic	Ohmic	Kinetic
N115	30 wt%	0.114	0.505	—	—	—	—	—	—
	50 wt%	0.129	0.526	—	—	—	—	—	—
	60 wt%	0.140	0.582	—	—	—	—	—	—
N212	30 wt%	0.058	0.482	0.133	0.556	0.079	0.511	0.063 (500 mAcm^{-2})	0.409 (500 mAcm^{-2})
	50 wt%	0.059	0.466	—	—	0.127	0.459		
	60 wt%	0.059	0.469	—	—	—	—		
SDAPP	30 wt%	0.031	0.459	0.050	0.514	0.030	0.486	0.025 (500 mA cm^{-2})	0.382 (500 mA cm^{-2})
	50 wt%	0.030	0.452	0.050	0.488	0.026	0.490		
	60 wt%	0.020	0.475	0.059	0.481	0.025	0.540	0.054 (1000 mA cm^{-2})	0.424 (1000 mA cm^{-2})

A short-term stability test was performed for MEAs fabricated with the three different membranes. The MEAs were evaluated under an acid product concentration of 40 wt% at 500 mA cm^{-2} and 100 ºC to have an equal basis of comparison. Figure 9 shows the results of the nominal 100-h test. The MEA performance follows the expected trend with an initial cell potential of 0.66 V for SDAPP followed by 0.72 V for N212, and 0.82 V for N115. The N212 MEA shows no degradation in performance indicating that both the catalyst layers and the membranes were stable during this test. In contrast, the SDAPP MEA membrane shows an increase in voltage of 50 μV h^{-1}. The voltage increase is speculated to be due to the cyclic operation of the syringe pump in the test system. Because SDAPP allows higher water transport from the cathode, the stability test required the cell to be operated under dry anode conditions to achieve 40 wt% product acid. Since water was provided only to the cathode side, oscillations in water supply were observed every time the syringe pump refilled, in essence exposing the system to wet/dry cycles, which is detrimental to membrane stability [35, 36]. However, when water was supplied to both electrodes (as in the case of N212), the MEA was not exposed to wet and dry cycles. In a separate experiment (not reported) an N212 MEA was operated under the same conditions used for the SDAPP MEA, producing 53 wt% acid. The resulting potential increase was measured at 90 μV h^{-1} indicating that the loss is mostly due to the wet and dry cycles from the syringe pump feeding water. In the case of the N115 MEA membrane, an increase of 300 μV h^{-1}

is observed. This loss can be attributed to catalyst deactivation as the operating potential of the N115 MEA is above 0.8 V. At high potentials, SO_2 adsorption competes with the formation of metal oxides, thereby deactivating the sulfur-modified catalyst [10, 16]. While this de-activation is temporary, the MEA will have to go through a break-in cycle to re-activate the catalyst layer.

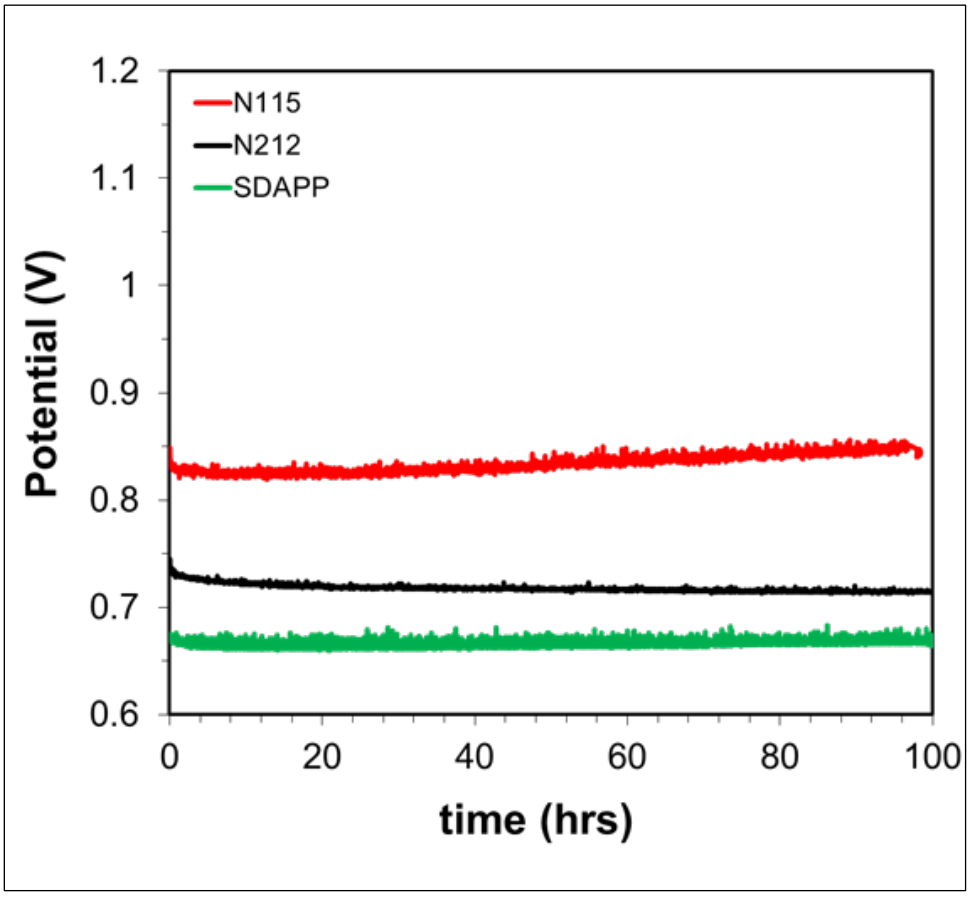

Figure 9. ***Short-term durability test for MEAs with N115, N212, and SDAPP membranes operated at 500 mA cm^{-2} and 100 ºC. Water flow at the cathode and anode was adjusted to produce a nominal acid concentration of 40 wt%.***

4.0 Conclusions

We evaluated the operation of a gas-fed SO_2-depolarized electrolyzer under different operating conditions using three different membranes with identical electrodes. The membranes were characterized for the amount of SO_2 transport through the membrane. Additionally, the electrodes were characterized by cyclic voltammetry to ensure all electrodes showed similar electrochemical surface area and the results were only influenced by the type of membrane. In general, the data showed that the lowest crossover was obtained

for N115 followed by SDAPP and N212 membranes. In all cases, the SO_2 crossover decreased with an increase in operating temperature. The electrolyzer performance evaluation was carried out by varying the amount of water fed and where (anode only, cathode only, or both) it was fed into the cell. We found that while the use of thinner membranes is beneficial in lowering the ohmic losses in the system, the acid concentration of the product stream is also lower due to an increase in water crossover. By changing where water is introduced into the electrolyzer, the product acid concentration can be increased while maintaining low ohmic overpotentials. Interestingly, with the use of a membrane with high water transport such as the SDAPP, both the ohmic and kinetic losses can be minimized while maintaining high acid concentration in the product. These results indicated that it is not only possible to operate at moderate potentials, but also that high acid concentrations can be achieved with proper membrane design. To the best of our knowledge, these results show the best SO_2-depolarized electrolysis performance at high and low acid concentrations operated under atmospheric conditions. Future work incorporating pressurized conditions and higher temperatures will further reduce kinetic overpotentials and should help approach the electrolyzer performance goals.

5.0 Acknowledgments

Financial support was provided by Savannah River National Laboratory's Laboratory Directed Research and Development and DOE-EERE Fuel Cell Technologies Office H2@SCALE Cooperative Research and Development program. Savannah River National Laboratory is managed and operated by Savannah River Nuclear Solutions, LLC under Contract No. DE-AC09-08SR22470 with the United States Government. Sandia National Laboratories is a multi-mission laboratory managed and operated by National Technology and Engineering Solutions of Sandia, LLC, a wholly owned subsidiary of Honeywell International, Inc., for the U.S. Department of Energy's National Nuclear Security Administration under contract DE-NA0003525.

6.0 References

1. Fuel Cells Technology Office, US Department of Energy. *H2@Scale: Enabling affordable, reliable, clean, and secure energy across sectors.* 2019; Available from: https://www.energy.gov/sites/prod/files/2019/09/f67/fcto-h2-at-scale-handout-2019.pdf.
2. Brecher, L. E., S. Spewock, and C. J. Warde, *The Westinghouse Sulfur Cycle for the thermochemical decomposition of water.* International Journal of Hydrogen Energy, 1977. **2**(1): p. 7-15.
3. Gorensek, M. B. and W. A. Summers, *Hybrid sulfur flowsheets using PEM electrolysis and a bayonet decomposition reactor.* International Journal of Hydrogen Energy, 2009. **34**(9): p. 4097-4114.
4. Gorensek, Maximilian B., Claudio Corgnale, and William A. Summers, *Development of the hybrid sulfur cycle for use with concentrated solar heat. I. Conceptual design.* International Journal of Hydrogen Energy, 2017. **42**(33): p. 20939-20954.
5. Gorensek, Maximilian B., Claudio Corgnale, John A. Staser, and John W. Weidner, *Solar Thermochemical Hydrogen (STCH) Processes.* The Electrochemical Society Interface, 2018. **27**(1): p. 53-56.
6. Lu, P. W. T., E. R. Garcia, and R. L. Ammon, *Recent developments in the technology of sulfur dioxide depolarized electrolysis.* Journal of Applied Electrochemistry, 1981. **11**(3): p. 347-55.
7. Lu, P. W. T. and R. L. Ammon, *Sulfur dioxide depolarized electrolysis for hydrogen production: development status.* International Journal of Hydrogen Energy, 1982. **7**(7): p. 563-75.
8. Lu, P. W. T., *Technological aspects of sulfur dioxide depolarized electrolysis for hydrogen production.* International Journal of Hydrogen Energy, 1983. **8**(10): p. 773-81.
9. Falch, A., V. Lates, and R. J. Kriek, *Combinatorial Plasma Sputtering of PtxPdy Thin Film Electrocatalysts for Aqueous SO2 Electro-oxidation.* Electrocatalysis, 2015. **6**(3): p. 322-330.
10. O'Brien, J. A., J. T. Hinkley, and S. W. Donne, *Electrochemical Oxidation of Aqueous Sulfur Dioxide II. Comparative Studies on Platinum and Gold Electrodes.* J. Electrochem. Soc., 2012. **159**(9): p. F585-F593.
11. Quijada, C., A. Rodes, J. L. Vazquez, J. M. Perez, and A. Aldaz, *Electrochemical-behavior of aqueous sulfur-dioxide at polycrystalline Pt electrodes in acidic medium - a voltammetric and in-situ FT-IR study .2. promoted oxidation of sulfur-dioxide - reduction of sulfur-dioxide.* J. Electroanal. Chem., 1995. **398**(1-2): p. 105-115.
12. Zelinsky, A. G., *Features of Sulfite Oxidation on Gold Anode.* Electrochimica Acta, 2016. **188**: p. 727-733.
13. Kriek, R. J., J. Rossmeisl, S. Siahrostami, and M. E. Bjorketun, *H-2 production through electro-oxidation of SO2: identifying the fundamental limitations.* Phys. Chem. Chem. Phys., 2014. **16**(20): p. 9572-9579.
14. Xue, L. L., P. Zhang, S. Z. Chen, and L. J. Wang, *Pt-based bimetallic catalysts for SO2-depolarized electrolysis reaction in the hybrid sulfur process.* International Journal of Hydrogen Energy, 2014. **39**(26): p. 14196-14203.
15. Colon-Mercado, H. R. and D. T. Hobbs, *Catalyst evaluation for a sulfur dioxide-depolarized electrolyzer.* Electrochem. Commun., 2007. **9**(11): p. 2649-2653.
16. Meekins, Benjamin H., Anthony B. Thompson, Varsha Gopal, et al., *In-situ and ex-situ comparison of the electrochemical oxidation of SO2 on carbon supported Pt and Au catalysts.* International Journal of Hydrogen Energy, 2020. **45**(3): p. 1940-1947.
17. Falch, A., V. A. Lates, H. S. Kotze, and R. J. Kriek, *The Effect of Rapid Thermal Annealing on Sputtered Pt and Pt3Pd2 Thin Film Electrocatalysts for Aqueous SO2 Electro-Oxidation.* Electrocatalysis, 2016. **7**(1): p. 33-41.
18. Falch, A., V. A. Badets, C. Labrugere, and R. J. Kriek, *Co-sputtered PtxPdyAlz thin film electrocatalysts for the production of hydrogen via SO2(aq) electro-oxidation.* Electrocatalysis, 2016. **7**(5): p. 376-390.

19. Huang, B. Y., Y. He, Z. H. Wang, et al., *Ru@Pt/C core-shell catalyst for SO2 electrocatalytic oxidation in electrochemical Bunsen reaction.* Electrochimica Acta, 2020. **331**.
20. Elvington, Mark C., Héctor Colón-Mercado, Steve McCatty, Simon G. Stone, and David T. Hobbs, *Evaluation of proton-conducting membranes for use in a sulfur dioxide depolarized electrolyzer.* Journal of Power Sources, 2010. **195**(9): p. 2823-2829.
21. Steimke, J. L., T. J. Steeper, H. R. Cólon-Mercado, and M. B. Gorensek, *Development and testing of a PEM SO2-depolarized electrolyzer and an operating method that prevents sulfur accumulation.* International Journal of Hydrogen Energy, 2015. **40**(39): p. 13281-13294.
22. Sivasubramanian, PremKumar, Ramaraja P. Ramasamy, Francisco J. Freire, Charles E. Holland, and John W. Weidner, *Electrochemical hydrogen production from thermochemical cycles using a proton exchange membrane electrolyzer.* International Journal of Hydrogen Energy, 2007. **32**(4): p. 463-468.
23. Staser, John A. and John W. Weidner, *Effect of Water Transport on the Production of Hydrogen and Sulfuric Acid in a PEM Electrolyzer.* Journal of The Electrochemical Society, 2009. **156**(1): p. B16.
24. Staser, J. A., K. Norman, C. H. Fujimoto, M. A. Hickner, and J. W. Weidner, *Transport properties and performance of polymer electrolyte membranes for the hybrid sulfur electrolyzer.* Journal of the Electrochemical Society, 2009. **156**(7): p. B842-B847.
25. Staser, John A., Maximilian B. Gorensek, and John W. Weidner, *Quantifying Individual Potential Contributions of the Hybrid Sulfur Electrolyzer.* Journal of The Electrochemical Society, 2010. **157**(6): p. B952.
26. Garrick, Taylor R., Cody H. Wilkins, Andrew T. Pingitore, et al., *Characterizing Voltage Losses in an SO2 Depolarized Electrolyzer Using Sulfonated Polybenzimidazole Membranes.* Journal of The Electrochemical Society, 2017. **164**(14): p. F1591-F1595.
27. Fujimoto, Cy H., Michael A. Hickner, Christopher J. Cornelius, and Douglas A. Loy, *Ionomeric Poly(phenylene) Prepared by Diels−Alder Polymerization: Synthesis and Physical Properties of a Novel Polyelectrolyte.* Macromolecules, 2005. **38**(12): p. 5010-5016.
28. Gorensek, M. B., J. A. Staser, T. G. Stanford, and J. W. Weidner, *A thermodynamic analysis of the SO2/H2SO4 system in SO2-depolarized electrolysis.* International Journal of Hydrogen Energy, 2009. **34**(15): p. 6089-6095.
29. Gorensek, Maximilian B., Benjamin Meekins, Héctor Colón-Mercado, and John Weidner, *Parametric study of operating conditions of an SO2-depolarized electrolyzer.* International Journal of Hydrogen Energy, 2020. **45**(43): p. 22408-22418.
30. Kaur, Harnoor, Meng Wang, Maximilian B. Gorensek, and Chau-Chyun Chen, *Thermodynamic modeling of the hybrid sulfur (HyS) cycle for hydrogen production.* Fluid Phase Equilibria, 2018. **460**: p. 175-188.
31. Gloaguen, F., J. M. Léger, and C. Lamy, *An electrochemical quartz crystal microbalance study of the hydrogen underpotential deposition at a Pt electrode.* J. Electroanal. Chem., 1999. **467**(1): p. 186-192.
32. Chen, C. H., A. Halford, M. Walker, et al., *Electrochemical characterization and regeneration of sulfur poisoned Pt catalysts in aqueous media.* J. Electroanal. Chem., 2018. **816**: p. 138-148.
33. Barique, M. A., E. Tsuchida, A. Ohira, and K. Tashiro, *Effect of Elevated Temperatures on the States of Water and Their Correlation with the Proton Conductivity of Nafion.* Acs Omega, 2018. **3**(1): p. 349-360.
34. Sorte, E. G., B. A. Paren, C. G. Rodriguez, et al., *Impact of Hydration and Sulfonation on the Morphology and Ionic Conductivity of Sulfonated Poly(phenylene) Proton Exchange Membranes.* Macromolecules, 2019. **52**(3): p. 857-876.
35. Kang, J. and J. Kim, *Membrane electrode assembly degradation by dry/wet gas on a PEM fuel cell.* International Journal of Hydrogen Energy, 2010. **35**(23): p. 13125-13130.

36. Mukundan, R., A. M. Baker, A. Kusoglu, et al., *Membrane Accelerated Stress Test Development for Polymer Electrolyte Fuel Cell Durability Validated Using Field and Drive Cycle Testing.* J. Electrochem. Soc., 2018. **165**(6): p. F3085-F3093.